Hybrid Au-CuO Nanoparticles: Effect of Structural Features for Selective Benzyl Alcohol Oxidation

Marcello Marelli,[†] Andrea Jouve,[†,‡] Alberto Villa,[†,‡] Rinaldo Psaro,[†] Antonella Balerna,[#] Laura Prati,[†,‡,*] Claudio Evangelisti,[†,*]

[†] CNR, Istituto di Scienze e Tecnologie Molecolari (ISTM), via C. Golgi 19, 20133 Milano, Italy.

[‡] Università degli Studi di Milano, via C. Golgi 19, 20133 Milano, Italy.

[#] Laboratori Nazionali di Frascati, INFN, Frascati, E. Fermi 40, Roma, Italy.

ABSTRACT: Hybrid Au-CuO NPs supported on carbon (Vulcan-XC72) with different Au/Cu molar ratios (i.e. 13/1, 4/1, 1/1 and 1/17) were synthesized by solvated metal atoms dispersion (SMAD) approach. (HR)-TEM, STEM-EELS maps and EXAFS measurements showed the presence of Au-CuO core-shell hetero-structure having narrow size distributions (mean diameter < 4.7 nm) regardless of their composition. The role of their structure and composition was evaluated for the catalytic liquid-phase selective benzyl alcohol oxidation with respect to their monometallic counterparts. As a result, a strong synergistic effect of Au-CuO heterostructure was revealed, strictly dependent on the CuO coverage degree of the Au-rich core and thus to the Au/Cu molar ratio. Highest catalytic activity was observed when CuO shell only partially cover the Au-NP surface (i.e. at high Au/Cu molar ratios: 13/1, 4/1). On the other hand, at high Cu loadings (i.e. Au/Cu molar ratios: 1/1 and 1/17), the CuO shell wraps completely the Au-core inhibiting the catalytic activity.

1. INTRODUCTION

Bimetallic nanoparticles (NPs) have received great interest over the last decade owing to their unique catalytic, optical, and magnetic features. The design of bimetallic NPs by advanced synthetic approaches offers an effective way to control their size, shape, composition and crystal structure which in turn are able to fine-tune their physicochemical properties[1]. NPs containing gold in the presence of another metal represents a new challenge in gold catalysis[2,3]. Among the promising metal pairs, Au and Cu metals are long-time friends: they are largely used together for coinage, jewellery or other technologic applications since could dissolve in one another in all proportions and they have similar chemistry[4]. Supported Au-Cu NPs as alloy or core-shell structures have been investigated pointing out at times a positive beneficial effect in terms of catalytic performances and stability respect to their monometallic counterparts[5]. In details, they were effectively used for the aerobic oxidation of carbon monoxide[6], oxidation of alcohols to the corresponding aldehydes or ketones[7,8,9,10] and propene epoxidation with nitrous oxide[11]. Recently, in order to disclose the essence of the synergistic effect between gold and copper in oxidation reactions, the structural evolution of supported Au-Cu alloy NPs in CO oxidation reaction has been deeply investigated by different research groups[12,13,14]. X. Liu et al. reported in situ studies about SBA-15 supported Au-Cu alloy NPs prepared through consecutive reductions of Au and Cu precursors. The active catalyst was composed by Au NPs enriched on the surface by partially or fully oxidized CuO_x tiny patches, which boosted the CO/O_2 activation[6,15]. J.C. Bauer et al. reported similar results with SiO_2-supported Au-Cu catalysts synthesized by adding copper acetate precursor to pre-formed supported Au NPs. The presence of Au-CuO_x hetero-structure significantly enhanced the catalyst performances. On the other hand, the formation of Au-Cu alloy, obtained after treatment of the catalysts under reductive conditions, led to a negligible CO conversion[16]. Finally, J. Yin et al. reported the CO oxidation promoted by carbon-supported $Au_{51}Cu_{49}$ catalysts, synthesized by bimetallic NPs impregnation. The reduction treatment by hydrogen of the calcined catalyst led to the formation of oxygenated Cu species at the NPs-surface, able again to activate oxygen affording a marked increase of the catalytic activity[17]. Despite experimental and theoretical efforts, the control of the copper surface segregation (i.e. the thickness of CuO on the surface) in Au-Cu alloy NPs under oxidative conditions and thus their behavior in catalytic oxidations is still a challenge. As a matter of facts, the degree of phase segregation is strongly influenced by the reaction conditions and oxidative/reductive pre-treatments, the substrates-metals interaction, the particles metal ratio as well as the synthetic approach. The selective oxidation of benzyl alcohol has attracted both academic and industrial interest because of the application of benzaldehyde in perfumery, dyestuff and agro-chemical industries[18,19,20]. Although the positive effect of the Cu on the Au-based catalysts for selective oxidation of benzyl alcohol was already reported[2,10,21], a correlation between the structural properties of the AuCu bimetallic NPs and their catalytic activity in this reaction still lacks.

Herein, we synthesized hybrid Au-CuO NPs supported on carbon (Vulcan XC-72) by solvated metal atoms dispersion (SMAD) for selective liquid-phase oxidation of benzyl alcohol to benzaldehyde. Recently, SMAD approach has been proposed as an effective way for the preparation of supported bimetallic Au-based and Cu-based NPs with high control of their size/composition, avoiding the use of any surfactant or capping

agent[22,23,24,25]. The morphological and structural features of SMAD-derived AuCu bimetallic catalysts containing different Au/Cu molar ratios were deeply investigated by HRTEM, STEM-EELS and EXAFS measurements, disclosing the role of the local particles- structure /-composition and their catalytic properties.

2. MATERIALS AND METHODS

2.1 Chemicals. Gold beads (1 - 6 mm, 99.999 %), copper powder (99.999 %) and acetone solvent were from Merck. Before the use, acetone was distilled and stored under argon. The co-condensation of copper, gold, and acetone vapors was carried out in a static metal vapor synthesis (MVS) reactor previously reported[26]. All operations involving the acetone-solvated Au-Cu atoms solutions were performed under a dry argon atmosphere by using standard Schlenk techniques. The VulcanXC-72 carbon support (graphitized carbon) was from Cabot (surface area: 218 m^2 g^{-1}, pore volume: 0.41 mL g^{-1}). Benzyl alcohol (puriss., meets analytical specification of Ph. Eur., BP, NF, 99-100.5% (GC)), O_2 from SIAD (99.99%) and cyclohexane (puriss. p.a. ACS reagent, ≥ 99.5%, GC) were from Sigma-Aldrich.

2.2 Synthesis of Carbon-supported Au-Cu catalysts. For the preparation of Au_4Cu_1/C sample, Au and Cu vapors were obtained by Joule heating of two alumina-coated tungsten crucibles, containing ca. 100 mg and 8 mg of Au beads and Cu powder, respectively. The metal vapors were co-condensed at -196°C (liquid nitrogen) with vapors of acetone (100 mL) into the MVS reactor for 1 hour. Thus, the reactor was warmed up until the solid matrix melting point (ca. -95°C) leading to a purple-brown solution (95 mL). The acetone-solvated Au-Cu atoms solution was then was siphoned at a low temperature (-40°C) into a Schlenk tube and kept in a refrigerator at -20°C. The Au and the Cu-contents of the AuCu-solvated metal atoms (SMA) solution were 0.52 mg mL^{-1} and 0.042 mg mL^{-1} for Au and Cu (Au/Cu molar ratio = 4:1), respectively, as determined by ICP-OES (Thermo Scientific ICAP6300 Duo) analysis. AuCu NPs were then quantitatively deposited onto Vulcan XC-72 carbon by adding 90 mL of the AuCu-SMA solution to a suspension of the support (5.1 g) in acetone (50 mL) under stirring at 25°C for 20 h. We separated the solution from the solid and collected the carbon-supported Au-Cu NPs after washing with *n*-pentane (50 mL, 3 times). Drying occurred under reduced pressure. The synthesis of the carbon-supported AuCu catalysts containing different Au/Cu molar ratios (13:1, 1:1 and 1:17) was carried out by the same procedure by varying the amount of copper powder used.

2.3 Instrumentation and Measurements. The SMAD-derived AuCu NPs were analyzed with Cs-aberration-corrected TEM. Samples were prepared dropping the acetone SMA solution onto supported ultra-thin film grids. HRTEM micrographs were collected by a Cs-image-corrected JEOL ARM200F, HRSTEM and STEM-EELS maps were collected by a Cs-Probe-corrected JEOL ARM200F equipped with a Gatan GIF Quantum ERS energy filter. Energy filtered maps were collected at energy loss 2239.0-2477.0eV for gold and 953.0-1202.0eV for copper. The supported AuCu/Carbon catalysts were prepared suspending the powder in isopropanol, sonicating the solution for 15 minutes and dropping it onto a holey-carbon supported film grid. The analysis was performed after complete solvent evaporation. TEM micrographs were collected by a ZEISS LIBRA200EFTEM instrument. Crystallographic data were processed by CrystBox Software[27]. ICP-OES analyzes were performed with a Thermofisher ICAP6200 Duo Upgrade with external calibration for Au and Cu contents. Samples for elemental analysis were acid digested with *aqua regia* and filtered on PTFE 0.2 μm filters.

The local atomic structure of the monometallic Au/C and bimetallic Au_xCu_y/C catalysts was studied using XAFS spectroscopy at the Cu K absorption edge and at the Au L_3 edge. Measurements were taken at the LISA beamline[28] of the European Synchrotron Radiation Facility (ESRF-Grenoble, France). When possible the XAFS spectra of the catalysts and of the reference samples (Au and Cu foils and CuO and Cu_2O oxides) at both edges were taken in transmission mode, otherwise the analysis were carried out in fluorescence mode using a 13-element high purity germanium solid state detector. The absorption coefficient was calculated as $\mu=\ln(I_0/I_T)$, in transmission mode, while as $\mu(E)=I_F/I_0$, in fluorescence mode. All X-ray absorption spectra were measured at -196°C (liquid nitrogen) in order to reduce the thermal effects. The sample powders were prepared as pellets adding some boron-nitride. The amounts of powder used for the different samples were calculated to achieve appropriate edge jumps[29]. The use of reference samples at both edges was necessary to calibrate the energy scales, to align the absorption spectra and to evaluate S_0^2 values[30]. Both near edge region (XANES) and extended x-ray absorption fine structure (EXAFS) were considered for the data analysis. EXAFS data, indicated as $\chi(k)$ (where k is the photoelectron wave vector[22]) were extracted using the ATHENA program[31] and the least-square parameter fitting was processed using the ARTEMIS program[31] both implemented in the IFEFFIT package[32]. Using the fitting procedure it was possible to determine the coordination numbers (N), the interatomic distances (R) and Debye-Waller factors (σ^2) of the coordination shells around the absorbing Cu and Au atoms. The fitting procedures of the reference samples and of many catalysts at the Au L_3 edge required single and multiple-scattering contributions, calculated using the FEFF6 software package[33]. At the Cu K edge, multiple scattering contributions were not included. In the analysis of all XAFS data, an estimation of the accuracy of the evaluated structural parameters, compatible with data quality and range[34] used, was taken into account.

2.4 Catalytic tests. The catalytic reactions were carried out in a thermostatic reactor (30 mL, glass) equipped with a magnetic stirrer and connected to a reservoir (5000 mL) filled with oxygen at 2 bar. The oxygen uptake was followed by a PC-drived mass flow controller, plotting a flow-time profile. The experiments were carried out using cyclohexane as solvent (0.15 M benzyl alcohol, substrate/metal= 500 mol/mol, 120 °C, pO_2=4 bar). The progress of the reaction was monitored by periodic removal of samples from the reactor. Mass recoveries were 98% ± 3%. The products were analyzed by a GC HP 7820A gas chromatograph with a capillary column (HP-5 30m x 0.32mm, 0.25 μm Film, Agilent Technologies). Reference samples were analyzed to determine separation times. Quantitative analysis were performed by external standard method (*n*-octanol).

The products were identified by a Trace ISQ QD Single Quadrupole GC-MS (Thermo Scientific) with a capillary column (HP-5 30 m x 0.32 mm, 0.25 x m Film, Agilent Technologies). The recycling tests were carried out using the recovered catalyst after filtration (recovery > 98%) in the subsequent run, without any further treatment.

3. RESULTS AND DISCUSSION

3.1 Synthesis and Characterization of Carbon-supported AuCu catalysts. We synthesized AuCu bimetallic catalysts deposited on Vulcan XC-72 carbon support by SMAD method. This approach allowed the synthesis of bimetallic NPs contained Au and Cu metals stabilized only by a weak-coordinative solvent (acetone) without the presence of additional stabilizers/ligands[35,36]. The Au_xCu_y NPs deposition onto the carbon support takes place as simple impregnation at 25°C in air. Differently, from classic colloidal impregnation, high-temperature post-process calcinations and/or activations steps (which can induce structural and morphological NPs modifications) are not required. Controlling the co-evaporation rate of Au and Cu metals, we prepared Au_xCu_y/Carbon catalysts containing different Au/Cu molar ratios (see Table 1). As comparison, we synthesized the corresponding carbon-supported Au and Cu monometallic systems.

Table 1. AuCu molar ratio (ICP-OES) and mean particle size (TEM) of the different Au_xCu_y/C samples

Sample	Molar ratio		Wt.% on C		Mean NPs Size (nm)
	Au	Cu	Au	Cu	
Au/C	1	0	1.0	0	2.7
$Au_{13}Cu_1$/C	13	1	0.98	0.02	3.5
Au_4Cu_1/C	4	1	0.93	0.07	4.5
Au_1Cu_1/C	1	1	0.75	0.25	4.7
Au_1Cu_{17}/C	1	17	0.15	0.85	3.5
Cu/C	0	1	0	1.0	2.9

The analysis of the size distribution and dispersion of the carbon-supported mono- and bimetallic NPs were carried out by conventional TEM (Figure S1 and S2). The mean NPs sizes of the different samples are summarized in Table 1. Concerning the monometallic catalysts, the analysis revealed a mean particle size of 2.7 nm and 2.9 nm for Au/C 1 wt. % and Cu/C 1 wt. %, respectively, as expected by previously reported analysis[37,38]. In both samples, their sizes lie in a narrow range (1 to 5 nm). Moving to the AuCu bimetallic catalysts, the mean values of the size distributions are slightly shifted to larger values than the ones found for monometallic systems (see Table 1 and Figure S1 and S2). The data pointing out that the co-presence of the two metals influenced the nucleation and growth processes of NPs. NPs sizes appeared meanly distributed in the 1 to 6 nm range even if in all the samples also a minor population of larger particles ranging from 7 to 12 nm was detected. In details, for the Au_4Cu_1/C and Au_1Cu_1/C samples, we observed a higher amount of larger NPs (less than 15 %) than that observed for the $Au_{13}Cu_1$/C and Au_1Cu_{17}/C samples (less than 5%).

In order to have a deep insight into the nature of bimetallic systems by their structural features, high resolution (HR)-TEM, STEM-EELS analysis and XAFS spectroscopy were carried out. The copper enriched sample (Au_1Cu_{17}/C) showed two different discrete systems: CuO_x NPs and Au-CuO_x core-shell structures (Figure 1a). It is worth noting that by SMAD approach both gold and copper metals are synthesized in their reduced state. However, the formation of CuO_x species after exposure in air atmosphere agrees with that previously reported data on SMAD-derived copper catalysts supported on carbon and it is ascribed to the high reactivity and the small size of the Cu NPs[37].

STEM-EELS maps clearly revealed that gold atoms tend to aggregate leading to Au-core NPs fully surrounded by a thin Cu enriched shell ranging from less than 1 nm to 3 nm depending on the whole particle size. As a matter of fact, the outer Cu-based shell appears strongly marked in the oversized NPs fraction but it is clearly present also in the mean size ones (Figure S3). The data agree with previously reported evidence on the surface segregation of CuO species derived from Au-Cu alloy NPs upon treatment under oxidative conditions[12,17].

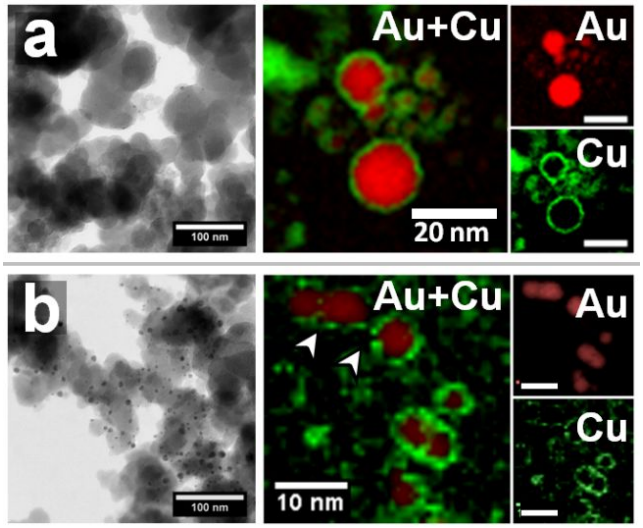

Figure. 1. Representative TEM micrograph (left side) and STEM-Energy filtered maps for Au and Cu - Au@2239.0-2477.0eV – Cu@ 953.0-1202.0eV – for a) Au_1Cu_{17}/C and b) Au_4Cu_1/C.

On the other hand, as observed in monometallic Cu/C sample and in the Cu maps, segregated CuO_x NPs ranging from 2 to 6 nm were detected. As estimated by TEM analysis on the supported sample (Figure S2), both Au-CuO_x and CuO_x NPs provide a metal size distribution centered around 3.5 nm.

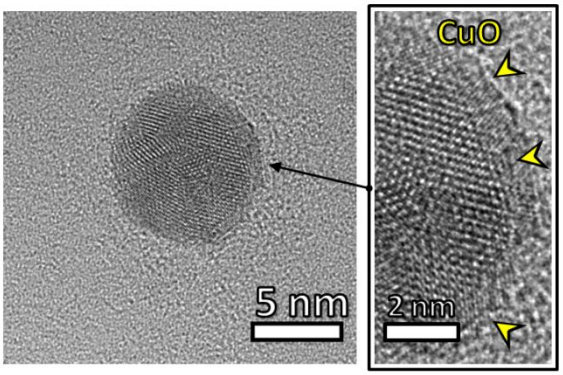

Figure 2. Representative (HR)-TEM-micrograph for Au_4Cu_1 sample: on the right, the arrows highlighted the CuO (023) crystalline planes.

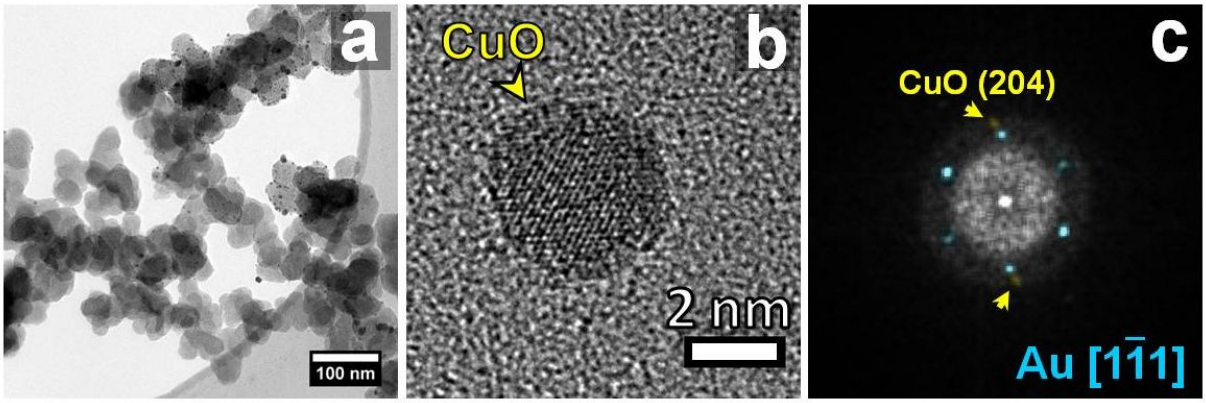

Figure 3. Representative TEM (a) and (HR)-TEM (b) micrographs for sample $Au_{13}Cu_1$/C.(c) The Fast Fourier Transform (FFT) of micrograph b shows the Au NP aligned along zone axis [1-11] and a reflex indexed as CuO (204).

Moving to the Au_4Cu_1 sample, STEM-EELS maps and (HR)-TEM analyzes highlighted NPs with the main size diameter of 4.5 nm (Figure 1b and Figure S2). Analogously to the previous sample, the copper is present on the NP-surface leading to Au-CuO_x hetero-structure where CuO_x partially covered the Au enriched cores. (HR)-TEM analysis confirmed the presence of the discontinued Cu-enriched outer shell, with visible segregated patches onto the Au core. Crystal planes could be indexed to the (023) CuO crystalline planes at 1.22 Å (Figure 2).

Finally, STEM-EELS maps on the $Au_{13}Cu_1$ sample (containing only the 0.02 Cu wt.%) were not able to reveal the fine structure of the NPs, whereas the presence of isolated CuO crystallites onto the Au NP surface (Figure 3) was observed by (HR)-TEM. FFT (Fast Fourier Transform) analysis revealed the presence of small segregated patches, ascribable to CuO crystalline plane (204) at 1.19 Å and clearly visible in figure 3b. We detected a main size diameter of 3.5 nm.

XAFS measurements and data analyzes were performed the Cu K edge and at the Au L_3 edge to define the present Cu oxide phase and to confirm the presence of an Au-core and Cu(II) like shell structure. In Figure 4 the XANES spectra of all the catalysts (Cu/C and Au_xCu_y/C) and of the Cu_2O and CuO reference samples are reported. The relevant similarities between the XANES spectra of the CuO reference sample and that of all catalysts show that Cu atoms in these samples are all in a Cu(II) phase confirming what found with STEM-EELS analysis.

The weak peak A, present in CuO and in the bimetallic and monometallic samples, is typical of Cu(II) compounds. While in Cu(I) compounds there are no holes in the *3d* orbitals, in Cu(II) ones, the presence of a d^9 configuration, gives the weak pre-edge absorption peak A, corresponding to a $1s \rightarrow 3d$ dipole forbidden but quadrupole allowed transition[37]. This weak peak represents the signature of the presence of divalent copper. Cu(II) compounds have also another important characteristic given by the higher energy values of their X-ray absorption edges compared to Cu(I) compounds. Also, this is clearly visible in Figure 4 taking into account that the positions of the B* peak of CuO reference sample and of the corresponding shoulders, present in the XANES spectra of the bimetallic and monometallic samples, are at a higher energy value compared to the B peak in Cu_2O. Of the three AuCu bimetallic catalysts the one with the higher amount of Cu, Au_1Cu_{17}/C, shows in the near edge region (see Figure 4) also the presence of a shoulder that, as already observed for other bimetallic AuCu and PdCu catalysts[16,25,39] has an energy position comparable to the one of the B peak in Cu_2O. This shoulder with lower intensity is also visible in the pre-edge region of the Cu/C sample. The absorption peak, B, is ascribed to the electric dipole-allowed $1s \rightarrow 4p$ transition, peculiar of Cu(I) ($3d^{10}$) compounds as Cu_2O having no holes in the *3d* orbitals. The shoulders present in these two catalysts, could indicate the presence of a small contribution coming from Cu(II) reduction, but this has no correspondent in the EXAFS data analysis that does not reveal the presence of O nearest neighbors at a distance comparable to the one of Cu(I) oxide compounds (R_1 = 1.85 Å)[37]. Since the intensity of this shoulder is higher in the bimetallic sample than in the monometallic one, the increase of its intensity could be related to a small Cu-Au contribution that giving a charge transfer from Au to Cu[39].

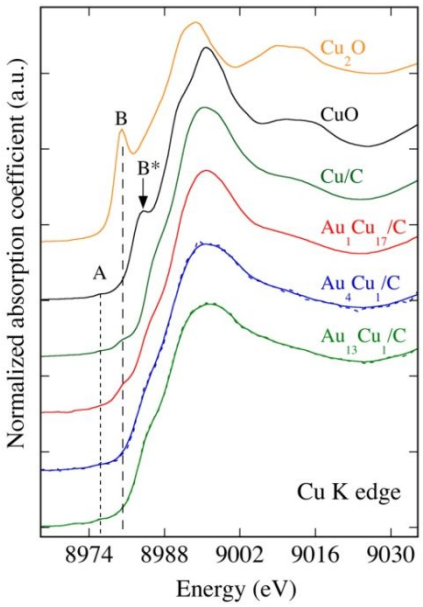

Figure 4. XANES spectra of the carbon-supported AuCu catalysts and of the Cu_2O and CuO reference samples. For the bimetallic systems with lower Cu amount, the solid lines represent the smoothed experimental data.

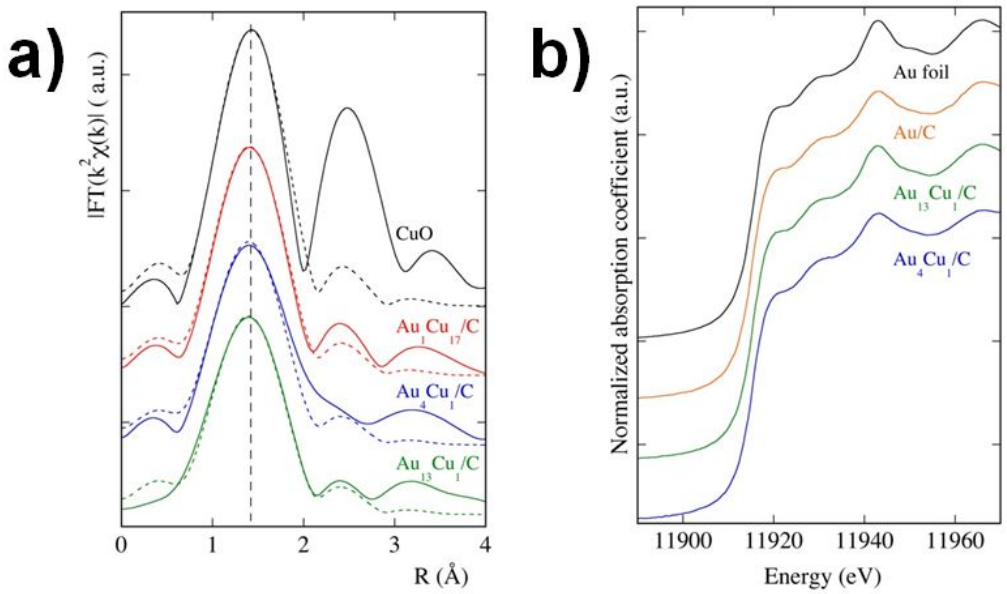

Figure 5. a) Fourier transforms (FT) of the experimental (solid lines) and theoretical (dashed lines) EXAFS spectra of the carbon-supported AuCu catalysts and of the CuO reference sample ($\Delta k = (2.5 - 7)$ Å^{-1}); b) XANES spectra of the monometallic Au/C and two of the bimetallic catalysts compared to the one of the Au foil reference sample.

Since the crystallographic structure of Cu(II) and Cu (I) compounds is quite different[37] we took into account the CuO and the Cu_2O reference samples. In Cu(II) compounds like CuO, copper is four-fold coordinated to O with a mean first shell coordination distance (R_1) of about 1.95 Å. Otherwise, in Cu (I) compounds like Cu_2O, copper atoms have as nearest neighbors two oxygen atoms at a distance of about 1.85 Å. As clearly visible in Figure S4 the Fourier Transforms spectra of the EXAFS data of the monometallic (N_1 = 3.8, R_1=1.937 Å) and of the bimetallic Au_1Cu_{17}/C (N_1= 3.6, R_1= 1.934 Å) samples are very similar and the position of their peaks corresponding to their first coordination shells are nearly that of the CuO reference sample (N_1= 4, R_1=1.95 Å). The small contraction of the Cu–O distance in the Cu/C sample compared to the value observed in the CuO reference sample could be ascribed to the small size of the NPs[40,41]. Due to very low amount of Cu in the other two bimetallic samples and to signal/noise ratio of the EXAFS data, the fitting procedure was limited to the first coordination shell with N and R values fixed to what found for the Au_1Cu_{17}/C sample due to the short usable k range ($\Delta k = (2.5 - 7)$ Å^{-1}). As shown in Figure 5a the first coordination shells of the bimetallic samples are practically all at the same position that is very similar but a bit shorter than that CuO. Due to the short usable EXAFS data range, it was not possible to investigate the presence of a possible second Cu-Au coordination shell in the samples with lower Cu amount. The XAFS data analysis of the catalysts at the Au L_3 edge revealed the presence of small Au NPs. As clearly visible in Figure 5b, the feature of Au white-line, centered at about 11920 eV in XANES spectra shows a slightly lower intensity in the bimetallic systems when compared to the Au reference sample. In gold bulk, the presence of this white line is ascribed to the *s-p-d* atomic level hybridization that gives a partial depletion of the filled $5d^{10}$ orbitals. The small Au NP size reduces this hybridization, leading to an increase of the 5*d* occupancy and therefore a reduction of the intensity of white-line[22,42]. Concerning the Au_1Cu_{17}/C sample, the one with the higher Cu amount, in this case (see Figure S5) an increase of the intensity of the white line was observed. Since the increase of this feature is related to the presence of *d*-holes, this effect confirms the charge transfer from Au to Cu, as evidenced also in the Cu K-edge data of this sample. As shown in Figure 6, the EXAFS data of the catalysts with the higher Au amount were fitted using an FCC structure and including multiple scattering contributions to fit also the higher coordination shells. Only for the Au_1Cu_{17}/C sample, due to the signal to noise ratio of the EXAFS data and having k_{max} = 8.0 Å^{-1} the fitting procedure was limited to the first coordination shell.

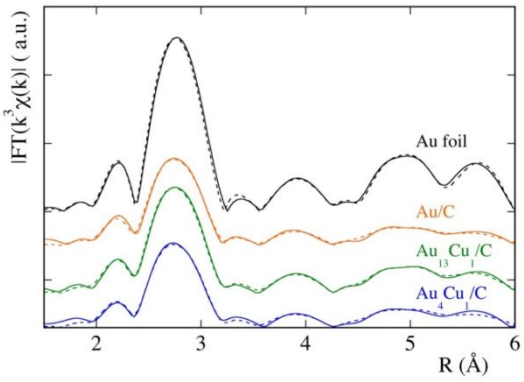

Figure 6. Fourier transforms (FT) of the experimental (solid lines) and theoretical (dashed lines) EXAFS spectra of the AuCu bimetallic systems compared to the one of Au foil reference sample ($\Delta k = (2.5 – 14.5)$ Å^{-1}).

Due to the Au NPs dimensions for the two samples with the higher Au amount, the EXAFS data analysis can confirm the presence of Au cores and, not finding any Au-Cu contribution, that Cu, as given by HRTEM analysis, could be confined in the outer shell around the Au-rich cores. In the case of the

Au_1Cu_{17}/C sample, EXAFS data analysis gives a contracted Au-Au first shell distance and a low coordination number (N_1= 8, R_1= 2.83 Å; N_{1bulk}=12, R_{1bulk}= 2.872Å) showing the presence of smaller Au-cores (Figure S6). The only effect of the Cu presence is given by the charge transfer from Au to Cu as shown in Figure S5. As detected by the STEM-EELS analysis probably only a part of the Cu atoms interacts with the surface atoms of these small Au-cores while the biggest amount contributes to the formation of a pure Cu(II) phase NPs taking into account the EXAFS data analysis at the Cu K edge.

3.2 Catalytic activity of Carbon-supported AuCu NPs. The efficiency of the catalysts was evaluated in the oxidation of benzyl alcohol (benzyl alcohol 0.15M, alcohol/metal = 500/1 mol/mol, 120 °C, pO_2 = 4 bar). Table 2 reports the catalytic activity (moles of reactant converted per hour per mol of metal) and the selectivity at 70% of reaction conversion.

Table 2. Catalytic Activity and Selectivity to Benzaldehyde

Catalyst[a]	Activity[b] (h^{-1})	Conversion (%) after 6h	Selectivity (%)[c]	
			Benzal-dehyde	Benzoic acid
Au/C	136	74	98	1
$Au_{13}Cu_1$/C	273	99	96	3
Au_4Cu_1/C	333	97	95	3
Au_1Cu_1/C	59	42	99[d]	-
Au_1Cu_{17}/C	0	0	-	-
Cu/C	0	0	-	-

a: Reaction conditions: benzyl alcohol 0.15 M, alcohol/metal = 500/1 mol/mol, 120 °C, pO_2 = 4 bar. b: Moles of reactant converted per hour per moles of metal (calculated at a reaction time of 30 min). c: Selectivity at 70% of conversion. d: Selectivity at 40% of conversion.

It can be observed that only Au/C, $Au_{13}Cu_1$/C, Au_4Cu_1/C and Au_1Cu_1/C are active under these reaction conditions, whereas Cu/C and Au_1Cu_{17}/C, did not show any activity. The best catalytic results were obtained using Au rich catalysts Au_4Cu_1/C (333 h^{-1}) and $Au_{13}Cu_1$/C (273 h^{-1}). Both samples exhibited a marked enhanced activity over the Au monometallic one (136 h^{-1}). Figure 7 shows a similar reaction profile for Au/C, $Au_{13}Cu_1$/C, Au_4Cu_1/C, Au_1Cu_1/C and no evident catalyst deactivation were observed. In the case of the $Au_{13}Cu_1$/C and Au_4Cu_1/C catalysts, almost full conversion was obtained after 6 h while monometallic Au/C reached 74 % of conversion. Noteworthy, the Au_1Cu_1/C catalyst showed significant low activity (42 % of conversion after 6 h) even though it exhibits a particle size distribution comparable with that of the $Au_{13}Cu_1$/C and Au_4Cu_1/C catalysts. Finally, the catalysts showed similar selectivity regardless of their different structural features, leading to high benzaldhehyde yields (selectivity 95-98 %, Table 2). In the case of Au rich catalysts, a small amount of benzoic acid (1-3 %) was detected. A particle size-effect on the catalytic performances of the Au-Cu bimetallic catalysts can be excluded based on the above-reported results. The behavior agrees with that previously reported for monometallic Au catalysts containing particles ranging 3-5 nm in size[43].

On the other hand, the data match with the beneficial and synergetic effect due to the co-presence of Au and segregated CuO at the NPs surface previously observed for gas-phase CO oxidation reaction[15,17]. It has been demonstrated that CO reacts with O_2 to produce CO_2 only when adsorbed on Au sites, whereas Cu species activate O_2 [15]. In particular, when CuOx partially covers the Au-rich core NPs, like for Au_4Cu_1/C and $Au_{13}Cu_1$/C, the reaction can occur at the Au-CuO interface. Otherwise, in the presence of a thick layer of CuOx, Au sites are not available and the reaction cannot proceed[15]. The enhanced performances of the hybrid Au-CuO bimetallic catalysts can be also ascribed to the synergic oxygen "spillover" effect previously invoked for other intermetallic precious metal/metal oxide composites, albeit for different catalytic reactions[44,45].

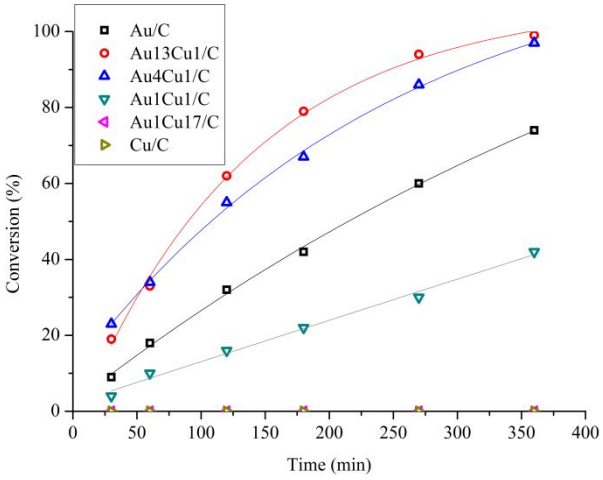

Figure 7. Conversion vs. time for Au and Cu catalysts.

Recycling tests have been performed using the most active catalyst, Au_4Cu_1/C showing good stability for 4 consecutive cycles (Figure S7). TEM analysis performed on the used catalyst (Figure S8) confirmed the stability of the catalyst showing a similar AuCu particle size than the fresh one (4.5 nm, Figure S2).

4. CONCLUSIONS

In summary, we synthesized by SMAD method a batch of Au-Cu bimetallic NPs supported on carbon (Vulcan-XC72) with different Au/Cu ratios and similar NPs sizes distributions. We observed by (HR)-TEM, STEM-EELS maps and EXAFS measurements the formation of hybrid Au-CuO core-shell NPs. The catalytic behavior of the bimetallic catalysts was evaluated in the selective benzyl alcohol oxidation carried out in liquid-phase, in order to explore the effect of the CuO structures on the Au-driven catalytic activity. As a result, the highest increase in the catalytic activity with respect to monometallic Au sample was observed for the catalysts containing low Cu loading, Au_4Cu_1/C and $Au_{13}Cu_1$/C (conversion after 6h of 97-99 %). In these samples, the segregated CuO segregates partially cover the Au-rich core of NP surface. On the other hand, when the CuO shell wraps completely the Au core (i.e. at high Cu loading, e.g. Au_1Cu_{17}/C) the reaction was completely inhibited.

The co-presence of Au and segregated CuO at the surface of the NPs plays a pivotal role in order to obtain a beneficial synergistic effect in AuCu bimetallic catalysts for liquid-phase alcohol oxidation. Finally, the reported results can effectively contribute to fine-tune the catalytic properties of AuCu bimetallic catalysts in other chemical reactions.

ASSOCIATED CONTENT

This material is available free of charge via the Internet at http://pubs.acs.org.

TEM micrographs and related size distribution, STEM EELS map, EXAFS and XANES spectra

AUTHOR INFORMATION

Corresponding Author

*E-mail: laura.prati@unimi.it
*E-mail:claudio.evangelisti@istm.cnr.it

ACKNOWLEDGMENT

MM would gratefully acknowledge the ESTEEM2 project for support through TA access to the Stuttgart Center for Electron Microscopy (StEM) - #20130318-Marelli.

REFERENCES

(1) Gilroy, K. D.; Ruditskiy, A.; Peng, H. C.; Qin, D.; Xia, Y. Bimetallic Nanocrystals: Syntheses, Properties, and Applications. *Chem. Rev.* **2016**, *116*, 10414–10472.

(2) Prati, L.; Villa, A.; Jouve, A.; Beck, A.; Evangelisti, C.; Savara, A. Gold as a Modifier of Metal Nanoparticles: Effect on Structure and Catalysis. *Faraday Discuss.* **2018**, *208*, 395-407

(3) Zugic, B.; Wang, L.; Heine, C.; Zakharov, D. N.; Lechner, B. A. J.; Stach, E. A.; Biener, J.; Salmeron, M.; Madix, R. J.; Friend, C. M. Dynamic Restructuring Drives Catalytic Activity on Nanoporous Gold–silver Alloy Catalysts. *Nat. Mater.* **2016**, *16*, 558–564.

(4) Fedorov, P. P.; Volkov, S. N. Au–Cu Phase Diagram. *Russ. J. Inorg. Chem.* **2016**, *61*, 772–775.

(5) Bracey, C. L.; Ellis, P. R.; Hutchings, G. J. Application of Copper–gold Alloys in Catalysis: Current Status and Future Perspectives. *Chem. Soc. Rev.* **2009**, *38*, 2231.

(6) Liu, X.; Wang, A.; Wang, X.; Mou, C.-Y.; Zhang, T. Au–Cu Alloy Nanoparticles Confined in SBA-15 as a Highly Efficient Catalyst for CO Oxidation. *Chem. Commun.* **2008**, *0* , 3187.

(7) Sugano, Y.; Shiraishi, Y.; Tsukamoto, D.; Ichikawa, S.; Tanaka, S.; Hirai, T. Supported Au-Cu Bimetallic Alloy Nanoparticles: An Aerobic Oxidation Catalyst with Regenerable Activity by Visible-Light Irradiation. *Angew. Chemie - Int. Ed.* **2013**, *52*, 5295–5299.

(8) Jia, Q.; Zhao, D.; Tang, B.; Zhao, N.; Li, H.; Sang, Y.; Bao, N.; Zhang, X.; Xu, X.; Liu, H. Synergistic Catalysis of Au-Cu/TiO2-NB Nano paper in Aerobic Oxidation of Benzyl Alcohol. *J. Mater. Chem. A* **2014**, *2*, 16292–16298.

(9) Li, W.; Wang, A.; Liu, X.; Zhang, T. Silica-Supported Au–Cu Alloy Nanoparticles as an Efficient Catalyst for Selective Oxidation of Alcohols. *Appl. Catal. A Gen.* **2012**, *433–434*, 146–151.

(10) Della Pina, C.; Falletta, E.; Rossi, M. Highly Selective Oxidation of Benzyl Alcohol to Benzaldehyde Catalyzed by Bimetallic Gold-Copper Catalyst. *J. Catal.* **2008**, *260*, 384–386.

(11) Llorca, J.; Domínguez, M.; Ledesma, C.; Chimentão, R. J.; Medina, F.; Sueiras, J.; Angurell, I.; Seco, M.; Rossell, O. Propene Epoxidation over TiO2-Supported Au-Cu Alloy Catalysts Prepared from Thiol-Capped Nanoparticles. *J. Catal.* **2008**, *258*, 187–198.

(12) Destro, P.; Kokumai, T. M.; Scarpellini, A.; Pasquale, L.; Manna, L.; Colombo, M.; Zanchet, D. The Crucial Role of the Support in the Transformations of Bimetallic Nanoparticles and Catalytic Performance. *ACS Catal.* **2018**, *8*, 1031–1037.

(13) Zhan, W.; Wang, J.; Wang, H.; Zhang, J.; Liu, X.; Zhang, P.; Chi, M.; Guo, Y.; Guo, Y.; Lu, G. et al. Crystal Structural Effect of AuCu Alloy Nanoparticles on Catalytic CO Oxidation. *J. Am. Chem. Soc.* **2017**, *139*, 8846–8854.

(14) Destro, P.; Marras, S.; Manna, L.; Colombo, M.; Zanchet, D. AuCu Alloy Nanoparticles Supported on SiO2: Impact of Redox Pretreatments in the Catalyst Performance in CO Oxidation. *Catal. Today* **2017**, *282*, 105–110.

(15) Liu, X.; Wang, A.; Li, L.; Zhang, T.; Mou, C.-Y.; Lee, J.-F. Structural Changes of Au–Cu Bimetallic Catalysts in CO Oxidation: In Situ XRD, EPR, XANES, and FT-IR Characterizations. *J. Catal.* **2011**, *278*, 288–296.

(16) Bauer, J. C.; Mullins, D.; Li, M.; Wu, Z.; Payzant, E. A.; Overbury, S. H.; Dai, S. Synthesis of Silica Supported AuCu Nanoparticle Catalysts and the Effects of Pretreatment Conditions for the CO Oxidation Reaction. *Phys. Chem. Chem. Phys.* **2011**, *13*, 2571.

(17) Yin, J.; Shan, S.; Yang, L.; Mott, D.; Malis, O.; Petkov, V.; Cai, F.; Shan Ng, M.; Luo, J.; Chen, B. H. et al. Gold-Copper Nanoparticles: Nanostructural Evolution and Bifunctional Catalytic Sites. *Chem. Mater.* **2012**, *24*, 4662–4674.

(18) Mallat, T.; Baiker, A. Oxidation of Alcohols with Molecular Oxygen on Solid Catalysts. *Chem. Rev.* **2004**, *104*, 3037–3058.

(19) Besson, M.; Gallezot, P. Selective Oxidation of Alcohols and Aldehydes on Metal Catalysts. *Catal. Today* **2000**, *57*, 127–141.

(20) Savara, A.; Chan-Thaw, C. E.; Sutton, J. E.; Wang, D.; Prati, L.; Villa, A. Molecular Origin of the

Selectivity Differences between Palladium and Gold–Palladium in Benzyl Alcohol Oxidation: Different Oxygen Adsorption Properties. *ChemCatChem* **2017**, *9*, 253–257.

(21) Wang, H.; Liu, D.; Xu, C. Directed Synthesis of Well Dispersed and Highly Active AuCu and AuNi Nanoparticle Catalysts. *Catal. Sci. Technol.* **2016**, *6*, 7137–7150.

(22) Evangelisti, C.; Schiavi, E.; Aronica, L. A.; Caporusso, A. M.; Vitulli, G.; Bertinetti, L.; Martra, G.; Balerna, A.; Mobilio, S. Bimetallic Gold–Palladium Vapour Derived Catalysts: The Role of Structural Features on Their Catalytic Activity. *J. Catal.* **2012**, *286*, 224–236.

(23) Bellini, M.; Folliero, M.G.; Miller, H.A.; Evangelisti, C.; He, Q.; Hu, Y.; Pagliaro, M.V.; Oberhauser, W.; Marchionni, A.; Fillipi, J. et al. A Gold-Palladium Nanoparticle Alloy Catalyst for CO Production from CO2 Electroreduction, *Energ. Tech.* **2018**, *in press*, doi: 10.1002/ente.201800859.

(24) Jouve, A.; Nagy, G; Somodi, F.; Tiozzo, C.; Villa, A.; Balerna, A.; Beck, A.; Evangelisti, C.; Prati, L. Gold-silver Catalysts: Effect of Catalyst Structure on The Selectivity of Glycerol Oxidation. J. Catal. **2018**, *368*, 324-335.

(25) Evangelisti, C.; Balerna, A.; Psaro, R.; Fusini, G.; Carpita, A.; Benfatto, M. Characterization of a Poly-4-Vinylpyridine-Supported CuPd Bimetallic Catalyst for Sonogashira Coupling Reactions. *ChemPhysChem* **2017**, *18*, 1921–1928.

(26) Evangelisti, C.; Schiavi, E.; Aronica, L. A.; Psaro, R.; Balerna, A.; Martra, G. In *Gold Catalysis: Preparation, Characterization, and Applications*; Prati, L., Villa, A., Eds.; Pan Stanford, 2015; pp 73–92.

(27) Klinger, M. More Features, More Tools, More CrysTBox. *J. Appl. Crystallogr.* **2017**, *50*, 1226–1234.

(28) D'Acapito, F.; Trapananti, A.; Puri, A. LISA: The Italian CRG Beamline for x-Ray Absorption Spectroscopy at ESRF. *J. Phys. Conf. Ser.* **2016**, *712*, 012021.

(29) Lee, P. A.; Citrin, P. H.; Eisenberger, P.; Kincaid, B. M. Extended X-Ray Absorption Fine Structure—its Strengths and Limitations as a Structural Tool. *Rev. Mod. Phys.* **1981**, *53*, 769–806.

(30) Rehr, J. J.; Albers, R. C. Theoretical Approaches to X-Ray Absorption Fine Structure. *Rev. Mod. Phys.* **2000**, *72*, 621–654.

(31) Ravel, B.; Newville, M. *ATHENA* , *ARTEMIS* , *HEPHAESTUS*: Data Analysis for X-Ray Absorption Spectroscopy Using *IFEFFIT*. *J. Synchrotron Radiat.* **2005**, *12*, 537–541.

(32) Newville, M. *IFEFFIT* : Interactive XAFS Analysis and *FEFF* Fitting. *J. Synchrotron Radiat.* **2001**, *8*, 322–324.

(33) Zabinsky, S. I.; Rehr, J. J.; Ankudinov, A.; Albers, R. C.; Eller, M. J. Multiple-Scattering Calculations of x-Ray-Absorption Spectra. *Phys. Rev. B* **1995**, *52*, 2995–3009.

(34) Li, G. G.; Bridges, F.; Booth, C. H. X-Ray-Absorption Fine-Structure Standards: A Comparison of Experiment and Theory. *Phys. Rev.B* **1995**, *52*, 6332–6348.

(35) Aronica, L.A.; Schiavi, E.; Evangelisti, C.; Caporusso, A.M.; Salvadori, P.; Vitulli, G.; Bertinetti, L.; Martra, G. Solvated Gold Atoms in the Preparation of Efficient Supported Catalysts: Correlation Between Morphological Features and Catalytic Activity in the Hydrosilylation of 1-hexyne. J. Catal. **2009**, 266, 250-257.

(36) Jumde, R.P.; Evangelisti, C.; Mandoli, A.; Scotti, N.; Psaro, R. Aminopropyl-silica-supported Cu Nanoparticles: An Efficient Catalyst for Continuous-flow Huisgen Azide-alkyne Cycloaddition (CuAAC). J. Catal. **2015**, *324*, 25-31.

(37) Balerna, A.; Evangelisti, C.; Tiozzo, C. XAFS Structural Characterization of Cu Vapour Derived Catalysts Supported on Poly-4-Vinylpyridine and Carbon. *X-Ray Spectrom.* **2017**, *46*, 82–87.

(38) Jouve, A.; Stucchi, M.; Barlocco, I.; Evangelisti, C.; Somodic, F.; Villa, A.; Prati, L. Carbon-Supported Au Nanoparticles: Catalytic Activity Ruled Out by Carbon Support. *Top. Catal.* **2018**, *18-19*, 1–11.

(39) Price, S. W. T.; Speed, J. D.; Kannan, P.; Russell, A. E. Exploring the First Steps in Core–Shell Electrocatalyst Preparation: In Situ Characterization of the Underpotential Deposition of Cu on Supported Au Nanoparticles. *J. Am. Chem. Soc.* **2011**, *133*, 19448–19458.

(40) Sharma, A.; Varshney, M.; Park, J.; Ha, T.-K.; Chae, K.-H.; Shin, H.-J. XANES, EXAFS and Photocatalytic Investigations on Copper Oxide Nanoparticles and Nanocomposites. *RSC Adv.* **2015**, *5*, 21762–21771.

(41) Comaschi, T.; Balerna, A.; Mobilio, S. Temperature Dependence of the Structural Parameters of Gold Nanoparticles Investigated with EXAFS. *Phys. Rev. B* **2008**, *77*, 075432.

(42) Balerna, A.; Bernieri, E.; Picozzi, P.; Reale, A.; Santucci, S.; Burattini, E.; Mobilio, S. Extended X-Ray-Absorption Fine-Structure and near-Edge-Structure Studies on Evaporated Small Clusters of Au. *Phys. Rev. B* **1985**, *31*, 5058–5065.

(43) Adnan, R.H.; Andersson, G.A.; Polson, M.I.J.; Method, G.F.; Golovko, V.B. Factors influencing the catalytic oxidation of benzyl alcohol using supported phosphine-capped gold nanoparticles. *Catal. Sci. Technol.*, **2015**, *5*, 1323-1333.

(44) Hu, S.; Goenaga, G.; Melton, C.; Zawodzinski, T.A.; Mukherjee, D. PtCo/CoOx nanocomposites: Bifunctional electrocatalysts for oxygen reduction and evolution reactions synthesized via tandem laser ablation synthesis in solution-galvanic replacement reactions. *Appl. Catal. B: Environ.* **2016**, *182*, 286-296.

(45) Sun, B.; Feng, X.; Yao Y.; Su, Q.; Ji, W.; Au, C-T. Substantial Pretreatment Effect on CO Oxidation over Controllably Synthesized Au/FeOx Hollow Nanostructures via Hybrid Au/β-FeOOH@SiO_2.

ACS Catal., **2013**, *3*, 3099-3105.

TOC Graphic